ACS Catalysis

pubs.acs.org/acscatalysis Letter

Bifunctional Metal–Organic Layer for Selective Photocatalytic Carbon Dioxide Reduction to Carbon Monoxide

Yingling Liao,[▽] Zitong Wang,[▽] Jinhong Li, Yingjie Fan, David Wang, Li Shi, and Wenbin Lin*

Cite This: *ACS Catal.* 2024, 14, 16957–16962 Read Online

ACCESS | Metrics & More | Article Recommendations | Supporting Information

ABSTRACT: We report a bifunctional metal–organic layer (MOL) as a photocatalyst for CO_2 reduction to CO under visible light irradiation with a turnover number of 6990 in 24 h and a CO selectivity of 99%. The fully accessible and modifiable Hf_{12} secondary building units and the coordinating porphyrin linkers of the MOL allow for the integration of both Ru photosensitizers and catalytic Fe-porphyrin sites into one single platform. The close distance (~11 Å) between the Ru photosensitizer and the catalytic center leads to enhanced electron transfer and promotes photocatalytic CO_2 reduction. This strategy leads to an increase of the CO_2-to-CO turnover number for the bifunctional MOL catalyst over a combination of a homogeneous Ru photosensitizer and an Fe-porphyrin complex. The mechanism of MOL-catalyzed CO_2 photoreduction was also studied by photophysical and electrochemical experiments.

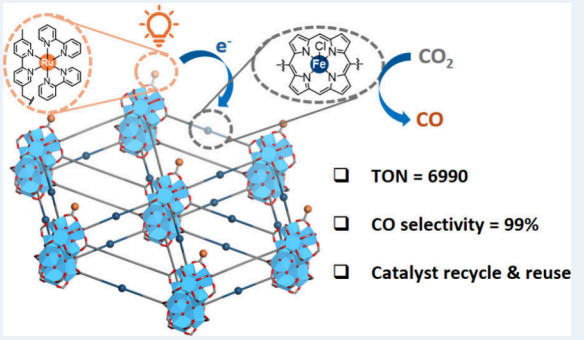

KEYWORDS: *metal–organic framework, two-dimensional materials, heterogeneous photocatalysis, CO_2 photoreduction, synergistic catalysis*

Photocatalytic carbon dioxide reduction (CO_2RR) to value-added products, such as carbon monoxide (CO), offers a promising approach for converting light energy into chemical energy and producing important chemical feedstocks.[1−3] In homogeneous systems, a light-harvesting photosensitizer and an active catalytic center are needed for photocatalytic CO_2RR. Upon light irradiation, the photosensitizer is excited and then reduced by a sacrificial reagent to form a reduced photosensitizer species, which transfers electron(s) to the catalytic center in solution to reduce CO_2 into desired fuels or chemical feedstocks.[3−8] The electron transfer process, a critical step in the catalytic cycle, is often sluggish due to the relatively low concentrations of both photosensitizers and catalytic centers, which significantly limits the efficiency of photocatalytic CO_2RR. To address this issue, researchers have focused on developing bifunctional homogeneous complexes by integrating both photosensitizing and catalytic components in the same molecular systems.[9,10] Despite their potential, these complexes are challenging to synthesize and cannot prevent multimolecular decomposition processes, which are accessible for highly reduced metal complexes.

Metal–organic frameworks (MOFs) are a family of crystalline porous molecular materials with periodic structures.[11−13] Postsynthetic modifications (PSMs) of MOFs allow for the introduction of various functional groups, making them outstanding candidates as heterogeneous catalysts.[14−46] For example, transition metal centers can be coordinated to functional linkers such as bipyridine (bpy) in the MOFs or incorporated into the preinstalled coordinating ligands on the secondary building units (SBUs).[47] However, the incorporation of multiple functional moieties into MOFs is often challenging. Incorporating relatively large photosensitizing species, such as $Ru(bpy)_3^{2+}$, into MOFs is also problematic due to their steric hindrance relative to MOF channels. These limitations have presented significant roadblocks to the development of MOFs as bifunctional photocatalysts. Recently, two-dimensional metal–organic layers have been developed as highly efficient photocatalysts due to their monolayered structures, which provide more accessible active sites.[48−54]

Here we report the rational design and construction of a two-dimensional (2D) metal–organic layer (MOL), **Hf-DBP-Fe/Ru**, as a bifunctional photocatalyst for CO_2RR. The Hf-DBP MOL, which was previously reported for nanomedicine applications, has porphyrin linkers as potential catalytic sites.[55,56] It was also reported that the capping monocarboxylate groups on the Hf_{12} SBUs can be replaced by other carboxylic-acid-containing functional groups.[56] Due to these advantages, the Hf-DBP MOL was first metalated with Fe(III) centers to form **Hf-DBP-Fe** by coordination of Fe(II) centers

Received: August 9, 2024
Revised: October 11, 2024
Accepted: October 24, 2024

https://doi.org/10.1021/acscatal.4c04772
ACS Catal. 2024, 14, 16957–16962

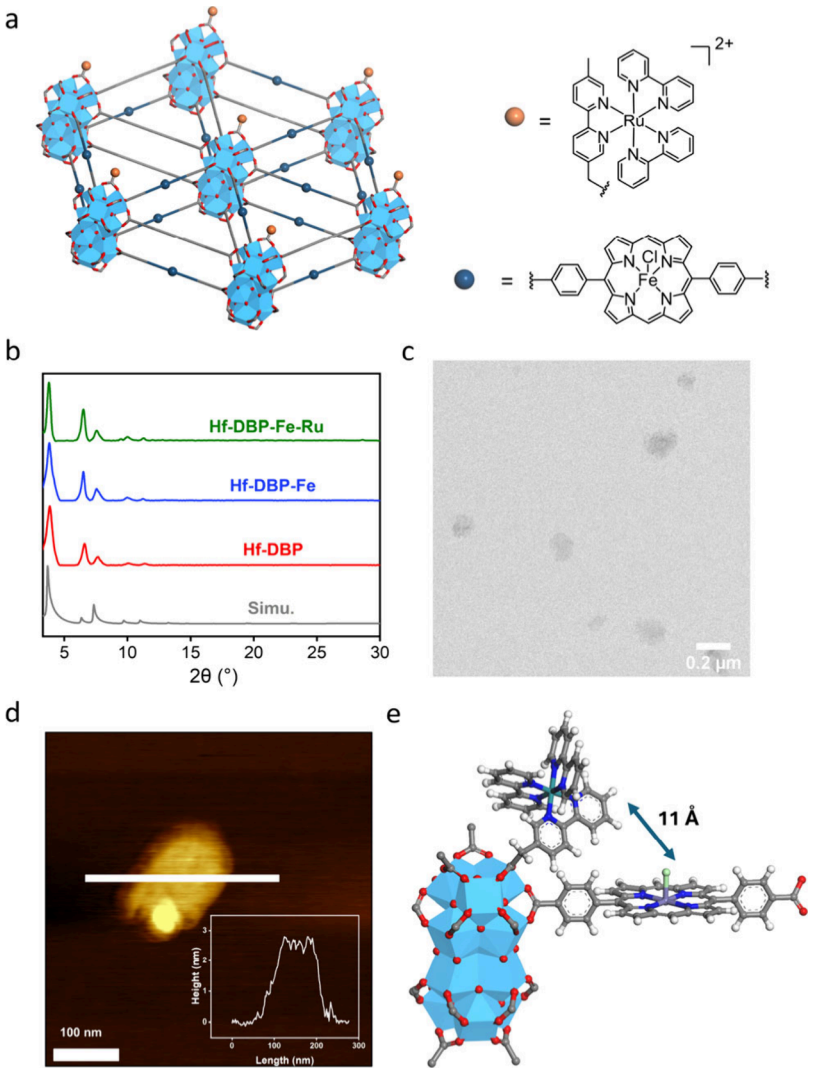

Figure 1. (a) Structural model of **Hf-DBP-Fe/Ru** MOL with photosensitizing Ru complexes and catalytic Fe sites; (b) PXRD patterns of **Hf-DBP** (red), **Hf-DBP-Fe** (blue), and **Hf-DBP-Fe/Ru** (green), as well as the simulated pattern (gray); (c) TEM images of **Hf-DBP-Fe/Ru**, showing a nanoplate morphology of ∼200 nm in diameter; (d) AFM image of **Hf-DBP-Fe/Ru**, showing a thickness of ∼3 nm; (e) scheme showing a Hf_{12} SBU with a $Ru(bpy)_3^{2+}$-type photosensitizer and a DBP-Fe catalytic center.

to the 5,15-di-*p*-benzoatoporphyrin (DBP) bridging ligands followed by air oxidation. The Hf_{12} SBUs in the **Hf-DBP-Fe** MOL were loaded with $Ru(bpy)_3^{2+}$-based monocarboxylate moieties via carboxylate exchange to form a bifunctional **Hf-DBP-Fe/Ru** MOL. **Hf-DBP-Fe/Ru** efficiently catalyzed photoreduction of CO_2 to CO under visible light irradiation with an outstanding turnover number of 6990 in 24 h and a high selectivity of 99%. Photophysical and electrochemical measurements revealed that DBP-Fe(II) catalytic sites readily accepted electrons from photoreduced Ru photosensitizers to generate DBP-Fe(I) centers for the CO_2 reduction. The proximity of photosensitizing $Ru(bpy)_3^{2+}$ moieties and catalytic Fe sites in **Hf-DBP-Fe/Ru** significantly accelerates their electron transfer, thereby enhancing the photoreduction of CO_2. The complete access to photosensitizing $Ru(bpy)_3^{2+}$ moieties and catalytic Fe sites in nonaggregating **Hf-DBP-Fe/Ru** MOL by dihydro-1*H*-benzo[*d*]imidazole (BIH) and CO_2, respectively, overcomes mass transfer limitations in related multifunctional MOF catalysts. As a result, **Hf-DBP-Fe/Ru** significantly outperformed the homogeneous control.

The **Hf-DBP** MOL was synthesized via a solvothermal reaction between $HfCl_4$ and H_2DBP in *N*,*N*-dimethylformamide (DMF) at 80 °C, with propionic acid (PA) as modulator.[55] During MOL growth, the propionates serve as capping groups to inhibit SBUs from connecting to each other by ditopic DBP ligands along the vertical direction. These Hf_{12} SBUs are linked by DBP ligands along the equatorial direction to generate a monolayered 2D network, with a chemical formula of $Hf_{12}(\mu_3\text{-}O)_8(\mu_3\text{-}OH)_8(\mu_2\text{-}OH)_6(DBP)_6(\mu_2\text{-}PA)_6$. The **Hf-DBP** MOL is well dispersed in various solvents, such as acetonitrile, ethanol, DMF, and water, without any precipitation or observable aggregation, which leads to excellent accessibility of postsynthetically installed active sites on the MOL. The **Hf-DBP** MOL was treated with trimethylsilyl trifluoroacetate (TMS-TFA) to completely replace capping propionates with trifluoroacetate (TFA) groups, which have much weaker binding with Hf centers in the SBUs compared to PA, allowing further modification of the SBUs with monocarboxyl-based functional moieties via carboxylate exchange.[56] ^1H NMR spectroscopy showed that no PA capping groups remained after the treatment of **Hf-DBP**

https://doi.org/10.1021/acscatal.4c04772
ACS Catal. 2024, 14, 16957−16962

with TMS-TFA (Figure S11). AFM images showed that TFA-capped **Hf-DBP** had a thickness of ∼1.8 nm, which is consistent with the expected thickness of a Hf_{12} SBU capped with six TFA groups (Figure S10).

Fe^{III} centers were coordinated to the DBP ligands by treating the TFA-capped **Hf-DBP** MOL with $FeCl_2$ in a mixture of acetonitrile and chloroform (2:1 v/v) followed by air oxidation to generate **Hf-DBP-Fe**. After this treatment, the purple dispersion of **Hf-DBP** turned brown, suggesting Fe coordination to DBP ligands in **Hf-DBP-Fe**. Inductively coupled plasma-mass spectrometry (ICP-MS) showed a Hf to Fe ratio of 3:1 in **Hf-DBP-Fe**, indicating 66% Fe occupancy in the DBP ligands. The TFA groups on the Hf_{12} SBUs of **Hf-DBP-Fe** were exchanged with the carboxylate-containing $Ru(bpy)_3^{2+}$ species, $(HMBA)Ru(bpy)_2Cl_2$ (HMBA is (5′-methyl-[2,2′-bipyridin]-5-yl)acetic acid), to construct the bifunctional MOL **Hf-DBP-Fe/Ru** (Figure 1a). UV−vis spectroscopy of the digested sample showed that 41% of TFA sites on Hf_{12}−SBUs were replaced by $(HMBA)Ru(bpy)_2Cl_2$ (Figure S21).

Powder X-ray diffraction (PXRD) experiments (Figure 1b) revealed that the crystallinity of the **Hf-DBP** MOL was retained after stepwise postsynthetic modifications. Transmission electron microscopy (TEM) images (Figure 1c) showed that the well dispersed MOLs exhibited a nanoplate morphology with a diameter of approximately 200 nm, which remained unchanged after Fe metalation and Ru-PS installation. High resolution TEM showed the lattice fringes of **Hf-DBP-Fe/Ru** to be around 3 nm, which is consistent with its lattice parameter (a = b = 2.8 nm) (Figure S14). Atomic force microscopy (AFM) showed a thickness of approximately 3 nm for **Hf-DBP-Fe/Ru**, which agrees well with the expected value after the SBUs are loaded with Ru-PSs and supports the monolayered structure of **Hf-DBP-Fe/Ru** (Figure 1d).

With both Ru-PSs and Fe catalytic sites on the MOL, the performance of **Hf-DBP-Fe/Ru** as a bifunctional CO_2RR photocatalyst was then tested. After optimization of the reaction conditions, *N*,*N*-dimethylacetamide (DMA) was selected as the solvent for the CO_2RR, and 1,3-dimethyl-2-phenyl-2,3-dihydro-1*H*-benzo[*d*]imidazole (BIH) was used as the sacrificial reductant. Irradiated by a xenon lamp with a 300 nm cutoff, **Hf-DBP-Fe/Ru** efficiently catalyzed CO_2 photoreduction, providing an excellent turnover number (TON) of 1567 in 5 h and a high CO selectivity of 99% (Figure 2a). After the CO_2 reduction reaction, only trace amounts of H_2 (TON = 11) and CH_4 (TON = 7) were detected as byproducts by gas chromatography (GC). While H_2 was produced by undesired competing reaction pathways, CH_4 likely resulted from further photoreduction of CO. Control experiments under a N_2 atmosphere showed negligible CO generation, excluding the possibility of CO generation from catalyst or solvent decomposition. Isotope labeling experiments using $^{13}CO_2$ as the carbon source verified that CO was generated from CO_2 reduction (Figure S18). Time-dependent CO_2RR experiments showed that the TON(CO) increased linearly during the reaction, suggesting that no catalyst decomposition or deactivation occurred under photocatalytic conditions. The TON of CO_2-to-CO conversion reached 6990 in 24 h (Figure 2b). Recycle tests demonstrated that the catalyst can be used in three consecutive runs without any decrease in CO generation and the crystallinity of the MOL was retained after the CO_2RR.

We conducted a series of control experiments with a mixture of homogeneous photosensitizers and Fe catalysts to assess the synergy between the loaded Ru-PSs and Fe catalytic sites on

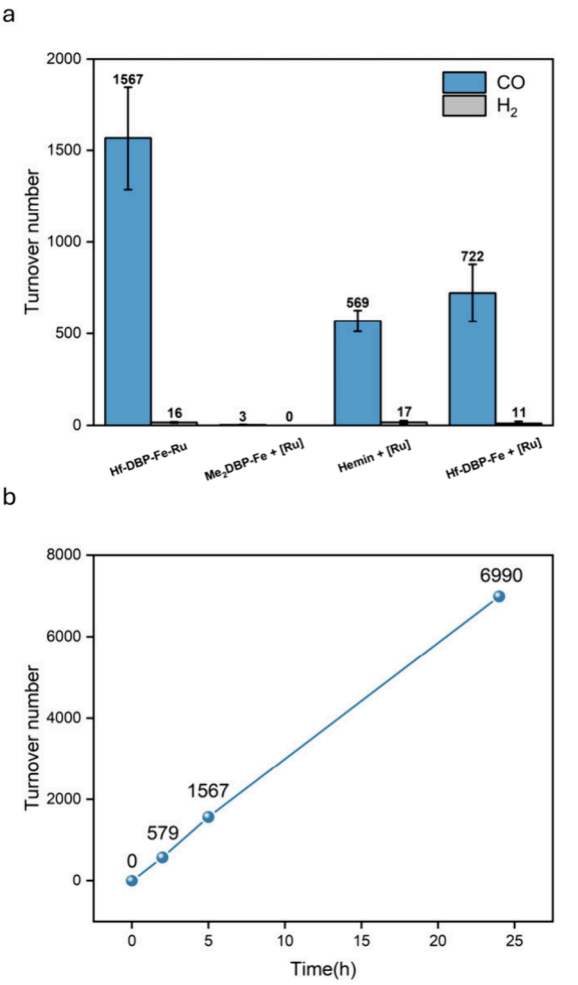

Figure 2. (a) Photocatalytic CO_2RR performance of **Hf-DBP-Fe/Ru**, Me_2DBP-Fe plus $(MeMBA)Ru(bpy)_2Cl_2$ ([Ru]), hemin plus [Ru], and **Hf-DBP-Fe** plus [Ru]. (b) Time-dependent CO_2RR experiments showing an unchanged CO generation rate in 24 h.

Hf-DBP-Fe/Ru. Under the same conditions, a combination of Me_2DBP-Fe and $(MeMBA)_2Ru(bpy)_2Cl_2$ in solution produced a negligible amount of CO (TON = 3 in 5 h), which suggests ineffective electron transfer between $(MeMBA)_2Ru(bpy)_2Cl_2$ and Me_2DBP-Fe under photocatalytic conditions. We also determined the catalytic performance of a combination of **Hf-DBP-Fe**, and homogeneous $(MeMBA)_2Ru(bpy)_2Cl_2$ and obtained a CO_2-to-CO TON of 722 in 5 h. We propose that the association between the homogeneous Ru-PS and completely accessible Fe sites on nonaggregating **Hf-DBP-Fe** may have facilitated the electron transfer process. Nonetheless, this TON was still less than half of the TON for **Hf-DBP-Fe/Ru**-catalyzed CO_2 photoreduction, which illustrates the advantage of loading both photosensitizing and catalytic moieties on a single material platform to construct a bifunctional photocatalyst. **Hf-DBP-Fe/Ru** catalyzes the CO_2RR more efficiently than the homogeneous controls via facilitating electron transfer between photosensitizing and catalytic components.

We conducted photophysical and electrochemical experiments to gain further insights into **Hf-DBP-Fe/Ru**-catalyzed CO_2 photoreduction. Luminescence quenching studies showed that the photoluminescence of $[(MeMBA)Ru(bpy)_2]Cl_2$ was significantly quenched by BIH, with a Stern−Völmer constant

https://doi.org/10.1021/acscatal.4c04772
ACS Catal. 2024, 14, 16957−16962

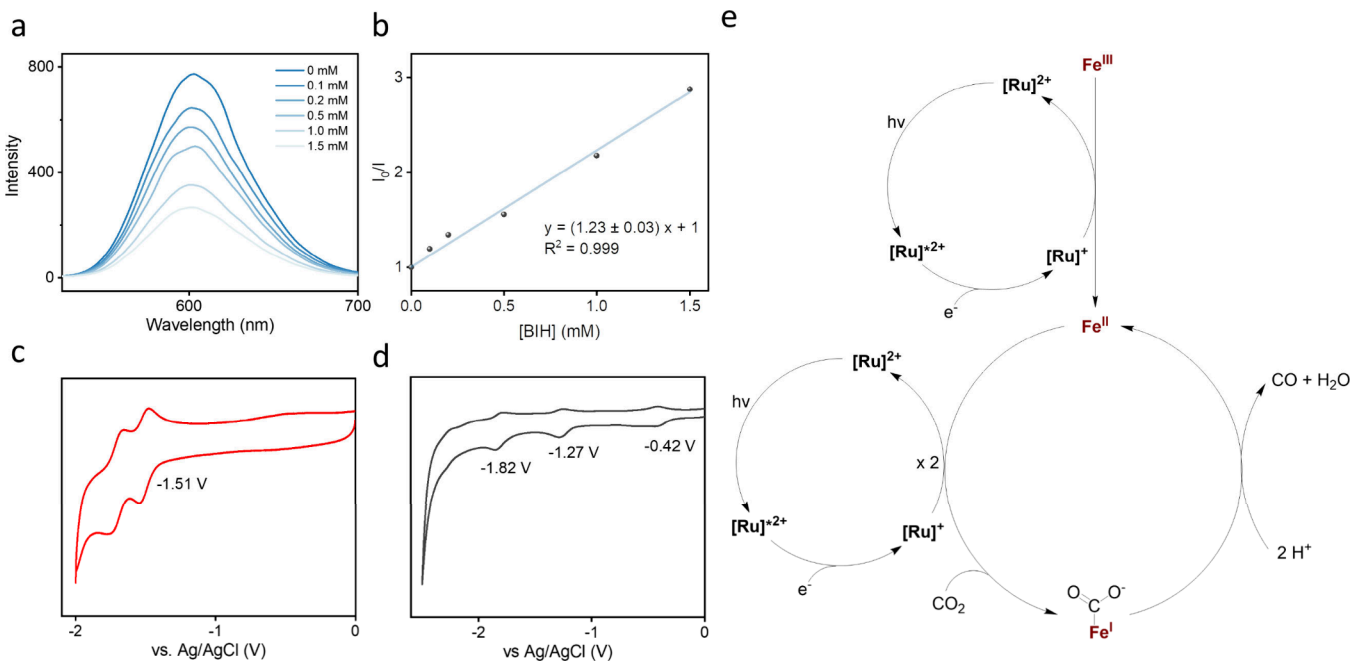

Figure 3. (a) Emission spectra of (MeMBA)Ru(bpy)$_2$Cl$_2$ (30 μM) after the addition of different amounts of BIH (from top to bottom: 0, 0.1, 0.2, 0.5, 1.0, 1.5 mM); (b) linear fitting of the photoluminescence quenching of (MeMBA)Ru(bpy)$_2$Cl$_2$ by BIH giving a Stern−Völmer quenching constant of 1.23 ± 0.03 mM^{-1}; (c, d) CV of (MeMBA)Ru(bpy)$_2$Cl$_2$ (c) and Me$_2$DBP-Fe (d); (e) proposed mechanism for the **Hf-DBP-Fe/Ru**-catalyzed CO_2RR with CO as the product.

of 1.23 ± 0.03 mM^{-1} (Figure 3a,b). This shows that the excited state of the Ru-PS ([Ru-PS]*) can be efficiently reduced by BIH to generate the highly reducing [(bpy$^{\cdot-}$)Ru(bpy)$_2$]$^+$ ([Ru]$^+$) species.[57] Cyclic voltammetry (CV) of [(MeMBA)Ru(bpy)$_2$]Cl$_2$ gave the redox potential of the bpy$^{0/-}$ pair of −1.51 V vs Ag/AgCl (Figure 3c). The CV of Me$_2$DBP-Fe exhibited three redox peaks at −0.42 V, −1.27 V, and −1.82 V for Fe$^{III/II}$, Fe$^{II/I}$, and Fe$^{I/0}$ pairs, respectively (Figure 3d). Thus, [Ru]$^+$ can reduce the Fe^{III} center in Fe-DBP to an Fe^{I} center which can react with CO_2 (with the input of another electron from [Ru]$^+$) to form an Fe^{I}(CO_2^-) intermediate. This is a key step in the CO_2-to-CO transformation. The Fe^{I}(CO_2^-) intermediate reacts with protons to form CO and H_2O while regenerating the Fe^{II} center to restart another catalytic cycle.[53] The close distance between the Ru-PS and Fe sites thus accelerates electron transfer to enhance the photocatalytic CO_2RR.

In summary, we developed a bifunctional MOL comprising both photosensitizing Ru(bpy)$_3^{2+}$ moieties and catalytic porphyrin-Fe centers for the photocatalytic CO_2RR. The 2D structure of the MOL allows ready access to the photosensitizing and catalytic sites during photocatalytic reactions. The proximity between photosensitizing Ru(bpy)$_3^{2+}$ moieties and catalytic Fe sites greatly facilitates electron transfer for CO_2 photoreduction, resulting in a greatly enhanced TON over a homogeneous control with a CO-selectivity of 99%. This work demonstrates MOLs as a novel molecular material platform to construct multifunctional catalysts for challenging transformations.

■ ASSOCIATED CONTENT

Supporting Information

The Supporting Information is available free of charge at https://pubs.acs.org/doi/10.1021/acscatal.4c04772.

Synthesis and characterization of complexes and materials; reaction procedures and characterization results of reaction products; procedures of mechanic studies (PDF)

■ AUTHOR INFORMATION

Corresponding Author

Wenbin Lin − *Department of Chemistry, The University of Chicago, Chicago, Illinois 60637, United States;* orcid.org/0000-0001-7035-7759; Email: wenbinlin@uchicago.edu

Authors

Yingling Liao − *Department of Chemistry, The University of Chicago, Chicago, Illinois 60637, United States; International Joint Research Center of Green Energy Chemical Engineering, East China University of Science and Technology, Shanghai 200237, China*

Zitong Wang − *Department of Chemistry, The University of Chicago, Chicago, Illinois 60637, United States;* orcid.org/0000-0001-7883-5276

Jinhong Li − *Department of Chemistry, The University of Chicago, Chicago, Illinois 60637, United States*

Yingjie Fan − *Department of Chemistry, The University of Chicago, Chicago, Illinois 60637, United States;* orcid.org/0000-0003-1857-5788

David Wang − *Department of Chemistry, The University of Chicago, Chicago, Illinois 60637, United States*

Li Shi − *International Joint Research Center of Green Energy Chemical Engineering, East China University of Science and Technology, Shanghai 200237, China;* orcid.org/0000-0002-2998-3384

Complete contact information is available at: https://pubs.acs.org/10.1021/acscatal.4c04772

https://doi.org/10.1021/acscatal.4c04772
ACS Catal. 2024, 14, 16957−16962

Author Contributions

[▽]Y. Liao and Z. Wang contributed equally.

Funding

This work was supported by NSF (CHE-2102554) and the University of Chicago.

Notes

The authors declare no competing financial interest.

REFERENCES

(1) Aresta, M.; Dibenedetto, A.; Angelini, A. Catalysis for the Valorization of Exhaust Carbon: from CO2 to Chemicals, Materials, and Fuels. Technological Use of CO2. *Chem. Rev.* **2014**, *114* (3), 1709−1742.

(2) Appel, A. M.; Bercaw, J. E.; Bocarsly, A. B.; Dobbek, H.; DuBois, D. L.; Dupuis, M.; Ferry, J. G.; Fujita, E.; Hille, R.; Kenis, P. J. A.; Kerfeld, C. A.; Morris, R. H.; Peden, C. H. F.; Portis, A. R.; Ragsdale, S. W.; Rauchfuss, T. B.; Reek, J. N. H.; Seefeldt, L. C.; Thauer, R. K.; Waldrop, G. L. Frontiers, Opportunities, and Challenges in Biochemical and Chemical Catalysis of CO2 Fixation. *Chem. Rev.* **2013**, *113* (8), 6621−6658.

(3) Berardi, S.; Drouet, S.; Francàs, L.; Gimbert-Suriñach, C.; Guttentag, M.; Richmond, C.; Stoll, T.; Llobet, A. Molecular artificial photosynthesis. *Chem. Soc. Rev.* **2014**, *43* (22), 7501−7519.

(4) Li, X.; Yu, J.; Jaroniec, M.; Chen, X. Cocatalysts for Selective Photoreduction of CO2 into Solar Fuels. *Chem. Rev.* **2019**, *119* (6), 3962−4179.

(5) Yamazaki, Y.; Takeda, H.; Ishitani, O. Photocatalytic reduction of CO2 using metal complexes. *Journal of Photochemistry and Photobiology C: Photochemistry Reviews* **2015**, *25*, 106−137.

(6) Zhang, B.; Sun, L. Artificial photosynthesis: opportunities and challenges of molecular catalysts. *Chem. Soc. Rev.* **2019**, *48* (7), 2216−2264.

(7) Rao, H.; Schmidt, L. C.; Bonin, J.; Robert, M. Visible-light-driven methane formation from CO2 with a molecular iron catalyst. *Nature* **2017**, *548* (7665), 74−77.

(8) Windle, C. D.; Perutz, R. N. Advances in molecular photocatalytic and electrocatalytic CO2 reduction. *Coord. Chem. Rev.* **2012**, *256* (21), 2562−2570.

(9) Kato, E.; Takeda, H.; Koike, K.; Ohkubo, K.; Ishitani, O. Ru(ii)−Re(i) binuclear photocatalysts connected by − CH2XCH2− (X = O, S, CH2) for CO2 reduction. *Chemical Science* **2015**, *6* (5), 3003−3012.

(10) Gholamkhass, B.; Mametsuka, H.; Koike, K.; Tanabe, T.; Furue, M.; Ishitani, O. Architecture of Supramolecular Metal Complexes for Photocatalytic CO2 Reduction: Ruthenium−Rhenium Bi- and Tetranuclear Complexes. *Inorg. Chem.* **2005**, *44* (7), 2326−2336.

(11) Furukawa, H.; Cordova, K. E.; O'Keeffe, M.; Yaghi, O. M. The Chemistry and Applications of Metal-Organic Frameworks. *Science* **2013**, *341* (6149), No. 1230444.

(12) Yaghi, O. M.; O'Keeffe, M.; Ockwig, N. W.; Chae, H. K.; Eddaoudi, M.; Kim, J. Reticular synthesis and the design of new materials. *Nature* **2003**, *423* (6941), 705−714.

(13) Kitagawa, S.; Kaskel, S.; Xu, Q. Metal-Organic Frameworks: Synthesis, Structures, and Applications. *Small Structures* **2022**, *3* (5), No. 2200072.

(14) Liang, Z.; Qu, C.; Xia, D.; Zou, R.; Xu, Q. Atomically Dispersed Metal Sites in MOF-Based Materials for Electrocatalytic and Photocatalytic Energy Conversion. *Angew. Chen., Int. Ed.* **2018**, *57* (31), 9604−9633.

(15) Bavykina, A.; Kolobov, N.; Khan, I. S.; Bau, J. A.; Ramirez, A.; Gascon, J. Metal−Organic Frameworks in Heterogeneous Catalysis: Recent Progress, New Trends, and Future Perspectives. *Chem. Rev.* **2020**, *120* (16), 8468−8535.

(16) Rogge, S. M. J.; Bavykina, A.; Hajek, J.; Garcia, H.; Olivos-Suarez, A. I.; Sepúlveda-Escribano, A.; Vimont, A.; Clet, G.; Bazin, P.; Kapteijn, F.; Daturi, M.; Ramos-Fernandez, E. V.; Llabrés i Xamena, F. X.; Van Speybroeck, V.; Gascon, J. Metal−organic and covalent organic frameworks as single-site catalysts. *Chem. Soc. Rev.* **2017**, *46* (11), 3134−3184.

(17) Wang, Z.; Yeary, P.; Fan, Y.; Deng, C.; Lin, W. Active Site Isolation and Enhanced Electron Transfer Facilitate Photocatalytic CO2 Reduction by A Multifunctional Metal−Organic Framework. *ACS Catal.* **2024**, *14* (12), 9217−9223.

(18) Zhuo, T.-C.; Song, Y.; Zhuang, G.-L.; Chang, L.-P.; Yao, S.; Zhang, W.; Wang, Y.; Wang, P.; Lin, W.; Lu, T.-B.; Zhang, Z.-M. H-Bond-Mediated Selectivity Control of Formate versus CO during CO2 Photoreduction with Two Cooperative Cu/X Sites. *J. Am. Chem. Soc.* **2021**, *143* (16), 6114−6122.

(19) Choi, K. M.; Kim, D.; Rungtaweevoranit, B.; Trickett, C. A.; Barmanbek, J. T. D.; Alshammari, A. S.; Yang, P.; Yaghi, O. M. Plasmon-Enhanced Photocatalytic CO2 Conversion within Metal−Organic Frameworks under Visible Light. *J. Am. Chem. Soc.* **2017**, *139* (1), 356−362.

(20) Yan, Z.-H.; Du, M.-H.; Liu, J.; Jin, S.; Wang, C.; Zhuang, G.-L.; Kong, X.-J.; Long, L.-S.; Zheng, L.-S. Photo-generated dinuclear {Eu(II)}2 active sites for selective CO2 reduction in a photosensitizing metal-organic framework. *Nat. Commun.* **2018**, *9* (1), 3353.

(21) Ming, M.-T.; Wang, Y.-C.; Tao, W.-X.; Shi, W.-J.; Zhong, D.-C.; Lu, T.-B. Designing dual-atom cobalt catalysts anchored on amino-functionalized MOFs for efficient CO2 photoreduction. *Green Chem.* **2023**, *25* (16), 6207−6211.

(22) Diercks, C. S.; Liu, Y.; Cordova, K. E.; Yaghi, O. M. The role of reticular chemistry in the design of CO2 reduction catalysts. *Nat. Mater.* **2018**, *17* (4), 301−307.

(23) Zhang, T.; Lin, W. Metal−organic frameworks for artificial photosynthesis and photocatalysis. *Chem. Soc. Rev.* **2014**, *43* (16), 5982−5993.

(24) Xu, H.-Q.; Hu, J.; Wang, D.; Li, Z.; Zhang, Q.; Luo, Y.; Yu, S.-H.; Jiang, H.-L. Visible-Light Photoreduction of CO2 in a Metal−Organic Framework: Boosting Electron−Hole Separation via Electron Trap States. *J. Am. Chem. Soc.* **2015**, *137* (42), 13440−13443.

(25) Cui, Y.; Yue, Y.; Qian, G.; Chen, B. Luminescent Functional Metal−Organic Frameworks. *Chem. Rev.* **2012**, *112* (2), 1126−1162.

(26) Cui, Y.; Li, B.; He, H.; Zhou, W.; Chen, B.; Qian, G. Metal−Organic Frameworks as Platforms for Functional Materials. *Acc. Chem. Res.* **2016**, *49* (3), 483−493.

(27) Feng, X.; Song, Y.; Lin, W. Transforming Hydroxide-Containing Metal−Organic Framework Nodes for Transition Metal Catalysis. *Trends Chem.* **2020**, *2* (11), 965−979.

(28) Kesanli, B.; Lin, W. Chiral porous coordination networks: rational design and applications in enantioselective processes. *Coord. Chem. Rev.* **2003**, *246* (1), 305−326.

(29) Drake, T.; Ji, P.; Lin, W. Site Isolation in Metal−Organic Frameworks Enables Novel Transition Metal Catalysis. *Acc. Chem. Res.* **2018**, *51* (9), 2129−2138.

(30) Huang, Y.-B.; Liang, J.; Wang, X.-S.; Cao, R. Multifunctional metal−organic framework catalysts: synergistic catalysis and tandem reactions. *Chem. Soc. Rev.* **2017**, *46* (1), 126−157.

(31) Liang, J.; Chen, R.-P.; Wang, X.-Y.; Liu, T.-T.; Wang, X.-S.; Huang, Y.-B.; Cao, R. Postsynthetic ionization of an imidazole-containing metal−organic framework for the cycloaddition of carbon dioxide and epoxides. *Chemical Science* **2017**, *8* (2), 1570−1575.

(32) Wu, Q.; Xie, R.-K.; Mao, M.-J.; Chai, G.-L.; Yi, J.-D.; Zhao, S.-S.; Huang, Y.-B.; Cao, R. Integration of Strong Electron Transporter Tetrathiafulvalene into Metalloporphyrin-Based Covalent Organic Framework for Highly Efficient Electroreduction of CO2. *ACS Energy Letters* **2020**, *5* (3), 1005−1012.

(33) Li, S.-L.; Xu, Q. Metal−organic frameworks as platforms for clean energy. *Energy Environ. Sci.* **2013**, *6* (6), 1656−1683.

(34) Yuan, K.; Liu, Z.; Yan, Z.; Yun, Q.; Song, T.; Guo, J.; Zhang, X.; Zhong, D.; Tang, Z.; Lu, T.; Hu, W. Metal−Organic Framework-Based Hetero-Phase Nanostructure Photocatalysts with Molecular-Scale Tunable Energy Levels. *Angew. Chen., Int. Ed.* **2024**, *63* (27), No. e202402693.

(35) Yang, W.; Wang, H.-J.; Liu, R.-R.; Wang, J.-W.; Zhang, C.; Li, C.; Zhong, D.-C.; Lu, T.-B. Tailoring Crystal Facets of Metal−

https://doi.org/10.1021/acscatal.4c04772
ACS Catal. 2024, 14, 16957−16962

Organic Layers to Enhance Photocatalytic Activity for CO2 Reduction. *Angew. Chen., Int. Ed.* **2021**, *60* (1), 409−414.
(36) Cao, C.-C.; Chen, C.-X.; Wei, Z.-W.; Qiu, Q.-F.; Zhu, N.-X.; Xiong, Y.-Y.; Jiang, J.-J.; Wang, D.; Su, C.-Y. Catalysis through Dynamic Spacer Installation of Multivariate Functionalities in Metal−Organic Frameworks. *J. Am. Chem. Soc.* **2019**, *141* (6), 2589−2593.
(37) Sun, Y.; Xue, Z.; Liu, Q.; Jia, Y.; Li, Y.; Liu, K.; Lin, Y.; Liu, M.; Li, G.; Su, C.-Y. Modulating electronic structure of metal-organic frameworks by introducing atomically dispersed Ru for efficient hydrogen evolution. *Nat. Commun.* **2021**, *12* (1), 1369.
(38) Luo, T.; Gilmanova, L.; Kaskel, S. Advances of MOFs and COFs for photocatalytic CO2 reduction, H2 evolution and organic redox transformations. *Coord. Chem. Rev.* **2023**, *490*, No. 215210.
(39) Huang, N.-Y.; Zheng, Y.-T.; Chen, D.; Chen, Z.-Y.; Huang, C.-Z.; Xu, Q. Reticular framework materials for photocatalytic organic reactions. *Chem. Soc. Rev.* **2023**, *52* (22), 7949−8004.
(40) Li, J.; Huang, H.; Xue, W.; Sun, K.; Song, X.; Wu, C.; Nie, L.; Li, Y.; Liu, C.; Pan, Y.; Jiang, H.-L.; Mei, D.; Zhong, C. Self-adaptive dual-metal-site pairs in metal-organic frameworks for selective CO2 photoreduction to CH4. *Nat. Catal.* **2021**, *4* (8), 719−729.
(41) Ma, X.; Liu, H.; Yang, W.; Mao, G.; Zheng, L.; Jiang, H.-L. Modulating Coordination Environment of Single-Atom Catalysts and Their Proximity to Photosensitive Units for Boosting MOF Photocatalysis. *J. Am. Chem. Soc.* **2021**, *143* (31), 12220−12229.
(42) Sun, K.; Qian, Y.; Jiang, H.-L. Metal-Organic Frameworks for Photocatalytic Water Splitting and CO2 Reduction. *Angew. Chen., Int. Ed.* **2023**, *62* (15), No. e202217565.
(43) Khan, I. S.; Mateo, D.; Shterk, G.; Shoinkhorova, T.; Poloneeva, D.; Garzón-Tovar, L.; Gascon, J. An Efficient Metal−Organic Framework-Derived Nickel Catalyst for the Light Driven Methanation of CO2. *Angew. Chen., Int. Ed.* **2021**, *60* (51), 26476−26482.
(44) Santaclara, J. G.; Olivos-Suarez, A. I.; Gonzalez-Nelson, A.; Osadchii, D.; Nasalevich, M. A.; van der Veen, M. A.; Kapteijn, F.; Sheveleva, A. M.; Veber, S. L.; Fedin, M. V.; Murray, A. T.; Hendon, C. H.; Walsh, A.; Gascon, J. Revisiting the Incorporation of Ti(IV) in UiO-type Metal−Organic Frameworks: Metal Exchange versus Grafting and Their Implications on Photocatalysis. *Chem. Mater.* **2017**, *29* (21), 8963−8967.
(45) Kutzscher, C.; Nickerl, G.; Senkovska, I.; Bon, V.; Kaskel, S. Proline Functionalized UiO-67 and UiO-68 Type Metal−Organic Frameworks Showing Reversed Diastereoselectivity in Aldol Addition Reactions. *Chem. Mater.* **2016**, *28* (8), 2573−2580.
(46) Wu, L.-Y.; Mu, Y.-F.; Guo, X.-X.; Zhang, W.; Zhang, Z.-M.; Zhang, M.; Lu, T.-B. Encapsulating Perovskite Quantum Dots in Iron-Based Metal−Organic Frameworks (MOFs) for Efficient Photocatalytic CO2 Reduction. *Angew. Chen., Int. Ed.* **2019**, *58* (28), 9491−9495.
(47) Wang, J.; Sun, K.; Wang, D.; Niu, X.; Lin, Z.; Wang, S.; Yang, W.; Huang, J.; Jiang, H.-L. Precise Regulation of the Coordination Environment of Single Co(II) Sites in a Metal−Organic Framework for Boosting CO2 Photoreduction. *ACS Catal.* **2023**, *13* (13), 8760−8769.
(48) Fan, Y.; Blenko, A. L.; Labalme, S.; Lin, W. Metal−Organic Layers with Photosensitizer and Pyridine Pairs Activate Alkyl Halides for Photocatalytic Heck-Type Coupling with Olefins. *J. Am. Chem. Soc.* **2024**, *146* (12), 7936−7941.
(49) Zheng, H.; Fan, Y.; Blenko, A. L.; Lin, W. Sequential Modifications of Metal−Organic Layer Nodes for Highly Efficient Photocatalyzed Hydrogen Atom Transfer. *J. Am. Chem. Soc.* **2023**, *145* (18), 9994−10000.
(50) Song, Y.; Pi, Y.; Feng, X.; Ni, K.; Xu, Z.; Chen, J. S.; Li, Z.; Lin, W. Cerium-Based Metal−Organic Layers Catalyze Hydrogen Evolution Reaction through Dual Photoexcitation. *J. Am. Chem. Soc.* **2020**, *142* (15), 6866−6871.
(51) Shi, W.; Quan, Y.; Lan, G.; Ni, K.; Song, Y.; Jiang, X.; Wang, C.; Lin, W. Bifunctional Metal−Organic Layers for Tandem Catalytic Transformations Using Molecular Oxygen and Carbon Dioxide. *J. Am. Chem. Soc.* **2021**, *143* (40), 16718−16724.
(52) Cao, L.; Wang, C. Metal−Organic Layers for Electrocatalysis and Photocatalysis. *ACS Cent. Sci.* **2020**, *6* (12), 2149−2158.
(53) Lan, G.; Fan, Y.; Shi, W.; You, E.; Veroneau, S. S.; Lin, W. Biomimetic active sites on monolayered metal−organic frameworks for artificial photosynthesis. *Nat. Catal.* **2022**, *5* (11), 1006−1018.
(54) Lan, G.; Quan, Y.; Wang, M.; Nash, G. T.; You, E.; Song, Y.; Veroneau, S. S.; Jiang, X.; Lin, W. Metal−Organic Layers as Multifunctional Two-Dimensional Nanomaterials for Enhanced Photoredox Catalysis. *J. Am. Chem. Soc.* **2019**, *141* (40), 15767−15772.
(55) Luo, T.; Fan, Y.; Mao, J.; Yuan, E.; You, E.; Xu, Z.; Lin, W. Dimensional Reduction Enhances Photodynamic Therapy of Metal−Organic Nanophotosensitizers. *J. Am. Chem. Soc.* **2022**, *144* (12), 5241−5246.
(56) Luo, T.; Fan, Y.; Mao, J.; Jiang, X.; Albano, L.; Yuan, E.; Germanas, T.; Lin, W. Metal-Organic Layer Delivers 5-Amino-levulinic Acid and Porphyrin for Dual-Organelle-Targeted Photodynamic Therapy. *Angew. Chen., Int. Ed.* **2023**, *62* (22), No. e202301910.
(57) McCusker, J. K. Femtosecond Absorption Spectroscopy of Transition Metal Charge-Transfer Complexes. *Acc. Chem. Res.* **2003**, *36* (12), 876−887.

https://doi.org/10.1021/acscatal.4c04772
ACS Catal. 2024, 14, 16957−16962